JOURNAL OF PROPULSION AND POWER
Vol. 17, No. 4, July–August 2001

Combustion Characteristics of a Liquid-Fueled Ramjet Combustor

Takao Inamura*
Hirosaki University, Hirosaki 036–8561, Japan
and
Mamoru Takahashi† and Akinaga Kumakawa‡
National Aerospace Laboratory, Kakuda 981-1525, Japan

The spray and combustion characteristics of a liquid-fueled ramjet combustor were experimentally analyzed. RJ-1J fuel was injected transversely into a subsonic hot vitiation airstream from a round injection orifice. The penetration of the liquid jet under hot airflow conditions was larger than that calculated by the empirical equation obtained under room-temperature airflow conditions. A V-shaped gutter was attached to the center of the combustor for flame holding. Two different arrangements of the gutter and the fuel injector were tested. In one, the fuel was injected perpendicular to the gutter axis, and in the other, the fuel was injected parallel to the axis. In regard to perpendicular fuel injection, a region with a temperature higher than 1500 K was observed at the center of the combustor; this region was long and narrow in the direction of the fuel injection. The high-temperature region reached the bottom wall due to involvement of the fuel in the wake region of the fuel injector and the liquid column. In regard to parallel injection, the high-temperature region covered the major part of the cross section of the combustor except in the vicinity of the bottom wall; the measured combustion efficiencies were higher than those for perpendicular fuel injection. Pilot fuel injection from the gutter was found to be a very effective method for improving combustion characteristics. In addition, it was found that the fuel dispersion in the direction of the injection of the high-temperature fuel, which simulates the regenerative cooling of a ramjet combustor, was lower than that of the low-temperature fuel due to fuel evaporation.

Nomenclature

d	=	fuel injector diameter
H	=	height from bottom combustor wall
H_n	=	distance from bottom combustor wall to exit of fuel injector
h	=	penetration of liquid jet in X direction
L	=	distance from center of fuel injector to windward edge of gutter in Z direction
$[O_2]$	=	oxygen mole concentration
P_s	=	static pressure
q	=	fuel-to-air momentum flux ratio
T_a	=	static air temperature
T_c	=	static temperature of combustion gas at combustor exit
T_f	=	fuel injection temperature
U_j	=	fuel injection velocity
V_a	=	air velocity in Z direction
X	=	distance from fuel injector exit in direction of liquid jet injection
Y	=	distance from center axis of combustor in direction perpendicular to X–Z plane
Z	=	distance from center of fuel injector exit in direction of airflow
Z_g	=	distance from leeward edge of gutter in Z direction
Z_h	=	distance from upstream side edge of fuel injector exit in direction of airflow, $(Z + d/2)$
η	=	combustion efficiency
ρ	=	density
σ	=	total pressure loss at combustor exit normalized by total pressure at inlet
ϕ	=	equivalence ratio

Subscripts

a	=	air
comp	=	complete combustion
in	=	representative at inlet
j	=	fuel jet
m	=	main fuel
meas	=	measurement
p	=	pilot fuel
t	=	total

Presented as Paper 96-2665 at the AIAA/ASME/SAE/ASEE 32nd Joint Propulsion Conference, Lake Buena Vista, FL, 1–3 July, 1996; received 19 March 1997; revision received 5 January 1998; accepted for publication 7 February 2001.

*Professor, Faculty of Science and Technology. Member AIAA.
†Researcher, Kakuda Research Center.
‡Head, Kakuda Research Center. Senior Member AIAA.

Introduction

STORABLE liquid fuel is attractive for use in the volume-limited ramjet engine, due to its high density and high heating value.[1] However, it requires evaporation and time to mix with air before ignition; insufficient evaporation and mixing result in low combustion efficiency and instability. On the other hand, liquid fuel can mix with combustion air because of its large inertia. Therefore, the disadvantages of liquid fuel may be compensated for by improving its spray characteristics and devising a means of mixing fuel droplets and combustion air.

As for the direction of fuel injection, transverse fuel injection into a high-speed airstream has been commonly used because it results in large penetration and thorough mixing between fuel droplets and air in comparison with parallel injection. Other researchers have studied the penetration and jet width of a traversing liquid jet in a supersonic airstream in regard to using these features in a supersonic combustion ramjet engine.[2–4] The penetration and jet width of a traversing liquid jet in the subsonic airstream have also been studied in regards to their use in the afterburners of gas turbine engines and liquid-fueled ramjet combustors.[5–9] Most data in the cited studies were obtained under room-temperature airflow conditions (cold flow conditions). However, the spray characteristics of a traversing

fuel jet under actual hot airflow conditions are very important for comparison with those obtained under cold flow conditions.

A V-shaped gutter is generally used due to low pressure loss and the high performance of the flame holding. In this paper, the conventional configuration of transverse fuel injection and a V-shaped gutter were employed. Here, the combustion characteristics depend on the combination of the direction of the fuel injection and that of the gutter axis. However, previous research has not clarified the effects of this combination on combustion characteristics.

Several researchers have examined the combustion characteristics of a liquid jet in a supersonic airflow,[10,11] as well as those of a gas-fueled ramjet engine.[12,13] However, there have been few studies on the combustion characteristics of a liquid-fueled ramjet engine.[14,15] The aim of the present series of studies is to clarify the relationship between the spray and the combustion characteristics of a liquid-fueled ramjet combustor.

In this study, penetrations of a liquid fuel jet into a hot airstream were measured and were compared with those under cold flow conditions. Firing tests of a ramjet combustor were carried out for the following two examples: one in which the liquid fuel was injected parallel to the gutter axis and the other in which the fuel was injected perpendicular to the axis. The combustion characteristics such as flame holding ability, temperature distributions, combustion efficiency, and total pressure loss were examined.

Experimental Apparatus and Conditions

The experimental apparatus is shown in Fig. 1. The ramjet combustor, which is made of stainless steel, has a rectangular cross section of 50 × 50 mm and a length of 563 mm. The fuel injector, which projects into the airstream, is attached to the bottom wall. The V-shaped gutter, the axis of which is perpendicular or parallel to the direction of liquid injection, is fixed at the center of the combustor. Static pressure taps are mounted on the upper wall in the direction of the airflow. Vitiation hot air, which is generated by mixing the air with a combustion gas of gaseous oxygen and hydrogen, passes through the combustor from left to right as is shown in Fig. 1. A jet of liquid fuel is injected transversely into the hot airstream. The exit of a gaseous oxygen/gaseous hydrogen torch igniter for ignition is located on the bottom wall just below the gutter; after ignition, the supply of oxygen/hydrogen is cut off. The distance between the exit of the fuel injector and the gutter in the direction of fuel injection is variable, and the distance between them in the direction of the airflow is also variable. The horizontal distance between the gutter and the exit of the combustor was maintained at 400 mm during all of the present experiments to avoid the effects of axial length of the combustor on combustion characteristics. For ease of observation, both of the side walls of the combustor can be replaced by crystal glass plates if necessary.

Figure 2 shows the fuel injector in detail. Three fuel injectors were used. They were made of stainless steel with inner diameters of 0.5, 0.7, and 1.0 mm. Each fuel injector has a length-to-diameter ratio of 9. The entrance of a straight passage with a diameter of d was polished so that no turbulent flow would take place. The vertical distance between the gutter and the injector exit was adjusted by rotating the fuel injector around its axis.

Figure 3 shows the configuration of the V-shaped gutter, which is made of stainless steel. The cross section of the gutter is triangular, and its blockage ratio is 0.2. Gaseous hydrogen fuel is ejected parallel to the airstream from 15 holes that are 0.5 mm in diameter on the leeward surface of the gutter. It was expected that gaseous hydrogen would act as a pilot fuel and would promote flame holding.

Figure 4 shows the sampling probe that was used to measure the total pressure and the components of the combustion gas. The sampling probe consists of nine copper pipes with an inner diameter of 0.7 mm. The copper pipes were cooled by impinging water jets. The components of the sampled combustion gas were measured by gas chromatography. The total pressure and components of the combustion gas in the cross section of the combustor were measured by horizontally traversing the sampling probe at the combustor exit.

Combustion efficiencies were calculated using the following equation:

$$\eta = [O_2]_{meas}/[O_2]_{comp} \tag{1}$$

where $[O_2]_{meas}$ indicates the measured value of the reductive quantity of O_2 mole concentration and $[O_2]_{comp}$ indicates the calculated value of the reductive quantity by complete combustion. $[O_2]_{meas}$ was measured by traversing the sampling probe at the combustor exit. The experimental uncertainties for oxygen mole concentration measurements were estimated to be less than 5% with an absolute value.

The temperatures of the combustion gas in the cross section of the combustor were measured at 5-mm intervals at the combustor exit by horizontally and vertically traversing an R-type thermocouple with a junction diameter of 0.5 mm. The effects of the radiation on the temperature measurements using the thermocouple were not

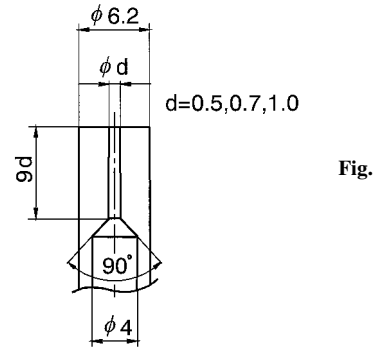

Fig. 2 Fuel injector.

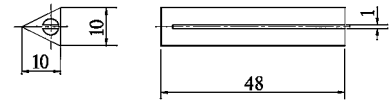

Fig. 3 V-shaped gutter.

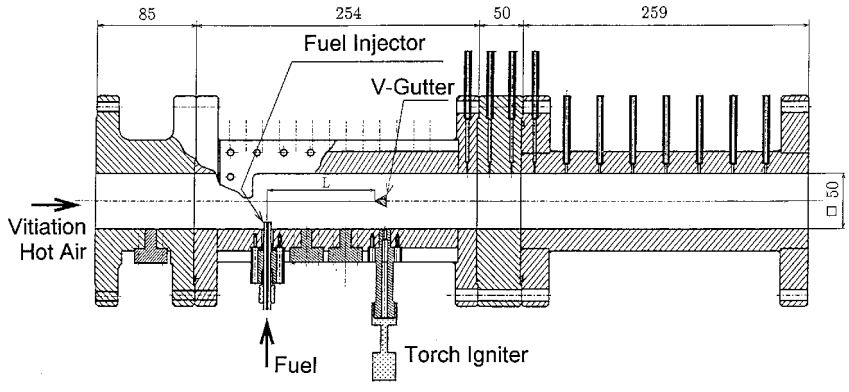

Fig. 1 Experimental apparatus.

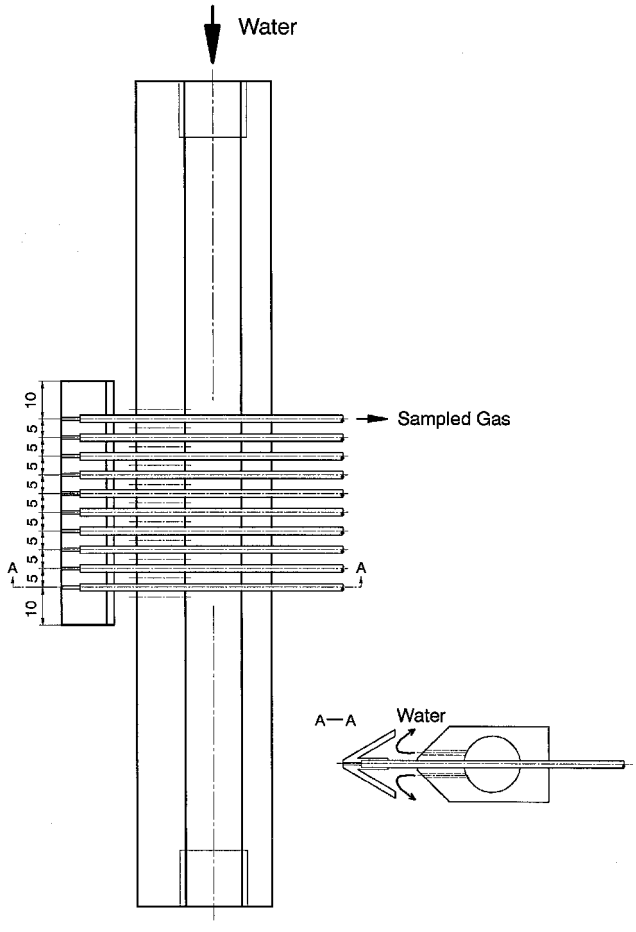

Fig. 4 Sampling probe.

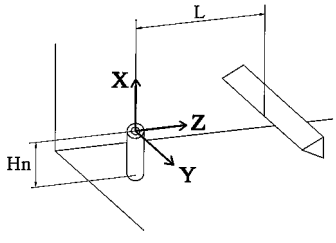

a) Perpendicular fuel injection

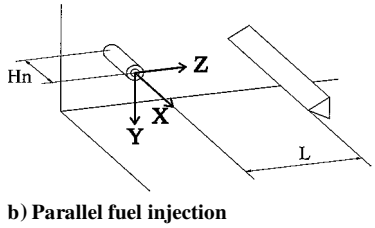

b) Parallel fuel injection

Fig. 5 Coordinate systems.

taken into account. Experimental uncertainties for temperature measurements were estimated to be less than 1%.

In this paper, two types of injections were examined: in one, fuel was injected parallel to the gutter axis, and in the other, fuel was injected perpendicular to the axis. Figures 5a and 5b show the coordinate systems that were used in those cases. H_n in Fig. 5 indicates the distance from the bottom combustor wall to the exit of the fuel injector.

Time-averaged photographs were taken to measure the penetration of a liquid jet with 1/60-s exposure time lighted from the rear top of a liquid jet. Black and white film (NEOPAN400, ASA400) was used to record the image. The images were digitized by a scanner,

Table 1 Thermophysical properties of RJ-1J fuel

Property	Value
Average chemical formulation	$C_{14}H_{26.8}$
Average molecular weight	194.8
Heat of formation (at 0.1 MPa, 298 K), J/mol	-398×10^3
Density (at 288 K), kg/m^3	851
Kinetic viscosity (at 293 K), m^2/s	4.0×10^{-6}
Surface tension (at 298 K), N/m	30.9×10^{-3}
Specific heat (at 293 K), J/kg · K	1.96×10^3
Heating value, J/kg	43.07×10^6

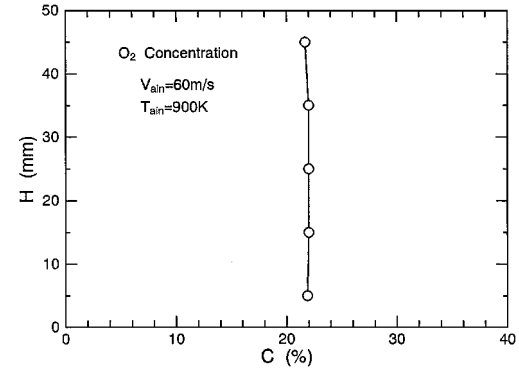

Fig. 6 Oxygen concentration profile of vitiation air at an inlet of the ramjet combustor.

and the boundary of the jet was determined by half of the maximum brightness of a jet. The accuracy of the penetration measurement was estimated to be about ±0.1 mm.

RJ-1J fuel, the physical properties and components of which are almost the same as those of RJ-1 fuel, was used for the combustion experiments. The thermophysical properties of RJ-1J fuel are shown in Table 1. The vitiation air temperature and the air velocity at the combustor inlet were 600 K and 100 m/s and 900 K and 60 m/s, respectively. Those values are equivalent to the expected flight Mach numbers of three and four, respectively. An extra experimental condition of 600 K and 60 m/s was added for comparison.

Figure 6 shows the oxygen concentration in the vitiation air. The oxygen concentration is uniform in the cross section of the combustor. The oxygen concentration in the vitiation air was controlled by adjusting the mixing ratio of the gaseous oxygen and hydrogen at generation; therefore, the oxygen concentration shown in Fig. 6 is almost the same as that in the air.

Figure 7 shows the distributions of the velocity and the temperature of vitiation air along the X axis at the combustor inlet. The velocity distribution is almost uniform except in the vicinity of the combustor wall. The boundary-layer thickness is estimated to be less than 5 mm based on 90% of the freestream velocity. With reference to the temperature distribution, the temperature gradually increases toward the upper wall of the combustor. This tendency decays for high-velocity conditions. Therefore, it was inferred that the nonuniformity of the air temperature could be ignored for high-velocity conditions in the present experiments.

The experimental uncertainties involved in setting up the representative air velocity and air temperature were less than ±5 m/s and ±20 K, respectively.

Jet Penetration in a Hot Airstream

Estimating the penetration of a fuel jet into an airstream is very important for ramjet combustor design. In a previous paper,[15] the authors deduced the empirical equation of jet penetration under cold flow conditions as follows:

$$h/d = (1.18 + 240d)q^{0.36} \times \ell n\{1 + (1.56 + 480d)Z_h/d\} \quad (2)$$

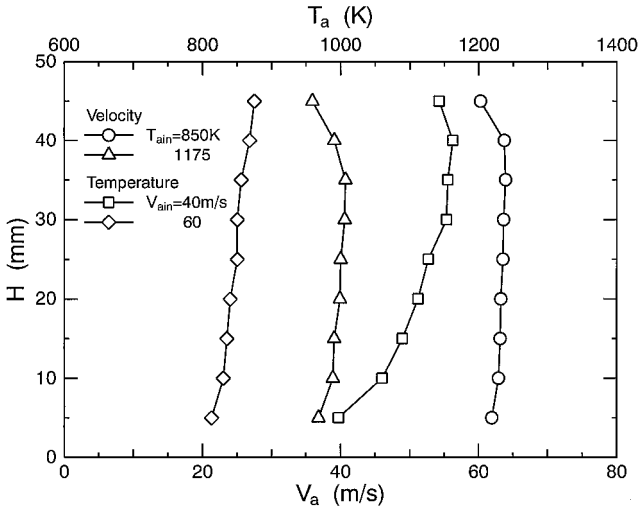

Fig. 7 Velocity and temperature distribution of vitiation air at an inlet of the ramjet combustor.

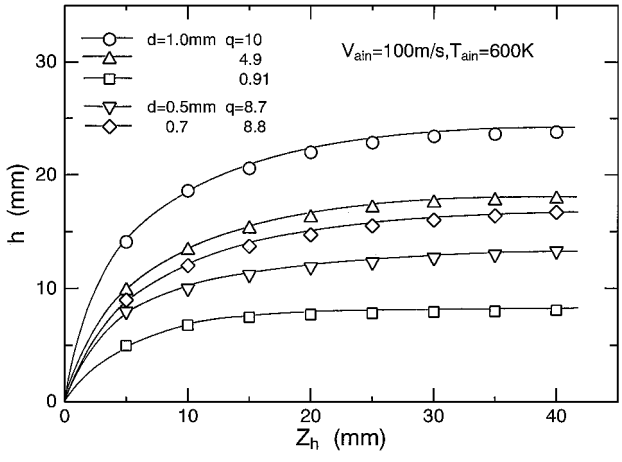

Fig. 8 Effects of fuel-to-air momentum flux ratio and fuel injector diameter on jet penetration.

where jet penetration was defined as the vertical distance from the bottom wall of the combustor to the outer edge of the fuel jet plume as measured by time-averaged photographs.

The jet penetration in a hot airstream was measured in the present study. Figure 8 shows the variations of the jet penetration in a hot airstream by the fuel-to-air momentum flux ratio and the fuel injector diameter. The jet penetration increased with an increase in the momentum flux ratio. The jet penetration increased rapidly in the vicinity of the injector exit and then gradually increased due to the increase of the drag of the airstream. The cross section of the jet is circular at the injector exit; it then becomes kidney shaped due to the dynamic pressure of the airstream.[4] This shape transformation results in an increase in the drag.

The liquid jet was disintegrated into liquid lumps due to the large-scale waves on the jet surface after the disturbance waves on the windward surface of the liquid jet grew to some extent along the jet's trajectory. The liquid lumps were disintegrated into finer droplets again due to aerodynamic force. The momentum of spray droplets in the direction of the liquid injection gradually decreased due to gravity and drag force, and in the direction of airflow, it increased due to the acceleration by airflow. Consequently, the penetration curve of the spray plume approached the airflow direction.

Figure 8 also shows the impact of fuel injector diameter on jet penetration. The larger the injector diameter is, the farther the fuel jet penetrates. The effects of injector diameter can be attributed to differences in the drag of the jet with unit volume by airflow. As the injector diameter decreases, the drag of the jet by the airstream

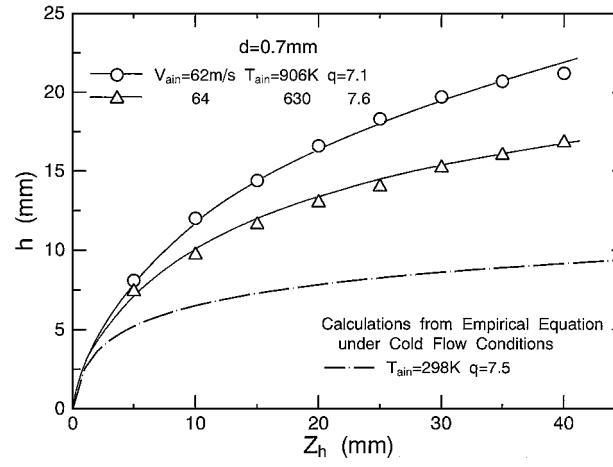

Fig. 9 Effects of static air temperature on jet penetration.

increases due to an increase in the frontal area per unit jet volume. The increase of drag reduces jet penetration. This tendency is similar to that under cold flow conditions.

Figure 9 shows the effects of static air temperature on the jet penetration. The dash–dotted line in Fig. 9 indicates the penetration as calculated from Eq. (2). Figure 9 shows that the penetrations in a hot airstream are much greater than those in a cold airstream. The increase in air temperature results in an increase of the jet penetration.

As for the evaporating droplets in a hot airstream, the evaporation of droplets results in a lowering of the drag force of the airstream.[16] In a similar fashion, evaporation lowers the drag of the evaporating liquid jet and increases its penetration. An increase in liquid temperature lowers its viscosity. Wu et al. pointed out that jet penetration decreases with an increase in liquid viscosity due to the increase in boundary-layer thickness in the liquid jet.[8] On the other hand, an increase in air temperature also lowers its density. Hsiang and Faeth showed that the Sauter mean diameter of the droplets generated by the second breakup of parent droplets is proportional to the liquid-to-gas density ratio to the one-fourth power.[17] Consequently, higher temperature air generates coarser droplets. Indeed, in this study many coarse droplets were observed in the high-temperature airstream rather than in the low-temperature airstream. A larger droplet penetrates farther than a smaller one due to larger inertia. However, they pointed out that additional measurements were needed to explore the effects of density ratio.

Jet penetration increases with an increase in the air temperature, probably due to the reasons mentioned earlier. However, data that indicate the effects of air temperature on jet penetration are limited, and further experiments should be done to clarify the effects of air temperature on jet penetration.

Maximum and Minimum Equivalence Ratios

Table 2 summarizes the maximum and minimum equivalence ratios using vitiation air where flame holding was confirmed and of parallel fuel injection under various experimental conditions with pilot hydrogen fuel injection. The pilot hydrogen fuel was always injected during measurement. The representative air velocity and temperature are those measured at the center of the combustor inlet. The experimental uncertainties for equivalence ratio calculations were estimated to be less than 4%. As will be discussed later, the combustion efficiency for perpendicular fuel injection is much lower than that for parallel fuel injection; the equivalence ratio range where flame holding is possible for perpendicular fuel injection was not studied in detail.

Comparison of $V_{a\,\mathrm{in}} = 100$ m/s and $T_{a\,\mathrm{in}} = 600$ K with $V_{a\,\mathrm{in}} = 60$ m/s and $T_{a\,\mathrm{in}} = 900$ K shows that the maximum and minimum equivalence ratios of the latter are far higher than those of the former. In the latter, the jet penetration is large due to high air temperature as already mentioned, and the mean diameter is also large due to low air velocity. Therefore, active fuel dispersion due to large jet

Table 2 Maximum and minimum equivalence ratios of parallel fuel injection

d, mm	L, mm	Maximum equivalence ratio	Minimum equivalence ratio
	$V_{a\,in} = 100$ m/s, $T_{a\,in} = 600$ K		
0.5	100	0.31	0.19
0.7	100	0.36	0.23
0.7	200	0.31	0.25
1.0	100	0.35	0.28
	$V_{a\,in} = 60$ m/s, $T_{a\,in} = 900$ K		
0.7	50	0.49	0.37
0.7	100	0.71	0.30
0.7	200	0.54	0.27
1.0	100	0.65	0.22
	$V_{a\,in} = 60$ m/s, $T_{a\,in} = 600$ K		
0.7	100	0.37	0.31
0.7	200	0.37	0.29

penetration and large inertia of large droplets occurs. In addition, active fuel dispersion causes the formation of a lean fuel/air mixture and results in higher maximum and minimum equivalence ratios.

Comparison of $V_{a\,\mathrm{in}} = 60$ m/s and $T_{a\,\mathrm{in}} = 900$ K with $V_{a\,\mathrm{in}} = 60$ m/s and $T_{a\,\mathrm{in}} = 600$ K shows that the minimum equivalence ratio of the former is slightly smaller than that of the latter. The maximum equivalence ratio of the former is much higher than that of the latter. As the air temperature decreases, the evaporation of fuel droplets becomes insufficient, and the equivalence ratio range where flame holding is possible consequently narrows.

For the type of the flame holder employed in this study, some fuel droplets collide on the surface of the gutter and form a fuel film there. The fuel film is disintegrated into spray droplets again at the leeward edge of the gutter. When it is considered that the 50% distillation point of RJ-1J fuel is about 520 K and assumed that the gutter surface temperature equals the inlet air temperature, the experimental conditions $V_{a\,\mathrm{in}} = 100$ m/s and $T_{a\,\mathrm{in}} = 600$ K and $V_{a\,\mathrm{in}} = 60$ m/s and $T_{a\,\mathrm{in}} = 900$ K seem to belong to the nucleate boiling and the film boiling regimes, respectively, in regard to fuel evaporation on the surface of the gutter. In the nucleate boiling regime, a thin liquid film can be easily generated by the collision of droplets with the surface of the gutter. On the other hand, in the film boiling regime, only a small amount of thin liquid film is generated. Here, note that the Leidenfrost point depends on various parameters, such as material and roughness of a solid wall, temperature and size of a droplet, and collision velocity of a droplet on a solid wall; therefore, the preceding statement is tentative.

Thus, under the condition that $V_{a\,\mathrm{in}} = 100$ m/s and $T_{a\,\mathrm{in}} = 600$ K, fine droplets can be easily generated at the leeward edge of the gutter by a high-speed airstream. However, under the condition that $V_{a\,\mathrm{in}} = 60$ m/s and $T_{a\,\mathrm{in}} = 900$ K, coarse droplets are generated at the leeward edge by a low speed airstream. These droplet formation mechanisms seem to influence the flammability range. However, because the present experimental results are limited, additional tests are needed to clarify the effects of droplet collision with the surface of the gutter on the flammability range in detail.

As concerns perpendicular fuel injection, the minimum equivalence ratio varies from 0.4 to 0.5 under all of the present experimental conditions and is much larger than that of the parallel fuel injection shown in Table 2. For perpendicular fuel injection, at a low equivalence ratio, the fuel cannot reach the gutter. This is why the minimum ratio is larger than that for parallel fuel injection.

Note that because the present equivalence ratio ranges were obtained using a small-scale wind tunnel and under special conditions using vitiation air, it is not certain whether these ranges are directly applicable to conditions in general.

Combustion Efficiencies

Table 3 summarizes the combustion efficiencies for various experimental conditions. Table 3 shows that the efficiencies of perpendicular fuel injection are lower than those of parallel fuel injection. For parallel fuel injection, the effects of the equivalence ratio on efficiency are small for no pilot fuel injection. However, the efficiency with pilot fuel injection is higher than that without it. Meanwhile, it was found from ignition experiments that pilot fuel injection makes flame holding much easier. Therefore, pilot fuel injection is very effective for improving combustion characteristics.

Table 3 Combustion efficiencies for various experimental conditions, L = 100

Air velocity and temperature	ϕ_m	ϕ_p	η
Perpendicular fuel injection			
$V_{a\,\mathrm{in}} = 100$ m/s, $T_{a\,\mathrm{in}} = 600$ K	0.57	0.01	0.61
$V_{a\,\mathrm{in}} = 60$ m/s, $T_{a\,\mathrm{in}} = 900$ K	0.59	0	0.76
Parallel fuel injection			
$V_{a\,\mathrm{in}} = 100$ m/s, $T_{a\,\mathrm{in}} = 600$ K	0.28	0.01	0.91
	0.38	0	0.70
$V_{a\,\mathrm{in}} = 60$ m/s, $T_{a\,\mathrm{in}} = 900$ K	0.47	0	0.73
	0.49	0.02	0.96
	0.42	0.02	(1.00)

Temperature Profiles in Cross Section

Direction of Fuel Injection

Figure 10 shows the temperature profile for the cross section under high inlet air velocity and low inlet air temperature conditions in the case of perpendicular fuel injection with pilot fuel injection. The broken lines in Fig. 10 indicate the contour of the gutter. The dash–dotted lines indicate the contour of the fuel injector. The temperature region that is higher than 1500 K is long and narrow in the direction of the fuel injection because the fuel vapor and droplets are pushed aside toward the upper or bottom walls along the surface of the gutter. The temperature significantly decreases toward the combustor walls. On the other hand, the temperature near the center of the bottom wall is very high. This is because the fuel vapor and fine fuel droplets are involved in the wake region of the fuel injector and the liquid column and some of them adhere to the bottom wall.

Figure 11 shows the temperature profile under high air velocity and low air temperature conditions for parallel fuel injection with pilot fuel injection. The temperature region that is higher than 1500 K is long on both sides in contrast with that for perpendicular fuel injection. Here, the fuel vapor and droplets are pushed aside toward the side walls due to the gutter. The high-temperature region is somewhat broader than that of perpendicular injection in spite of having a smaller equivalence ratio. In Fig. 10, the temperature region that is higher than 1500 K is about 30% of the combustor cross-sectional area, whereas in Fig. 11 it is about 38%. In the case of perpendicular fuel injection, the amount of fuel that collides with the gutter is limited. However, in the case of parallel fuel injection, most of the fuel collides with the gutter, and a moderate fuel/air mixture is formed downstream of it. Thus, this moderate mixture contributes to higher heat release.

As stated earlier, the high-temperature region of the parallel fuel injection is apparently broader than that of the perpendicular fuel injection, and the combustion efficiency of the former is higher than that of the latter, as shown in Table 3. Therefore, the following section on the results of combustion experiments are limited to parallel fuel injection with pilot fuel injection except for one example with a proviso.

Equivalence Ratio

Figure 12 shows the temperature profile under low air velocity and high air temperature conditions. The equivalence ratio of Fig. 12 is almost the same as that of Fig. 11. The maximum temperature in Fig. 12 is lower than that in Fig. 11. As already mentioned, the fuel dispersion of the former appears to be superior to that of the latter due to larger mean droplet size. Therefore, the maximum local equivalence ratio of the former is smaller than that of the latter. This causes the lower maximum temperature in Fig. 12. The slope of the

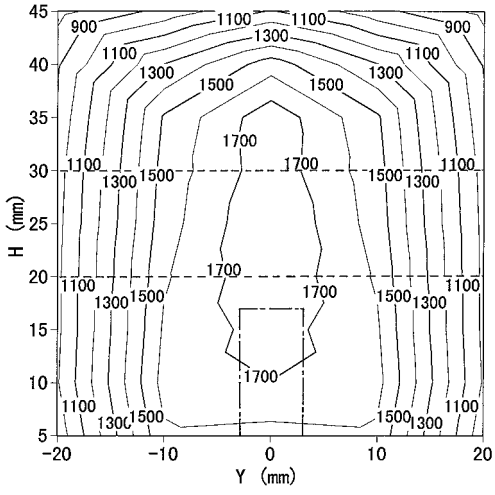

Fig. 10 Temperature profile under high air velocity and low air temperature conditions for perpendicular fuel injection with pilot fuel injection: $V_{a\,\mathrm{in}}$ = 100 m/s, $T_{a\,\mathrm{in}}$ = 600 K, ϕ_m = 0.57, q = 8.0, H_n = 17 mm, L = 100 mm, d = 1.0 mm, and T_f = 298 K.

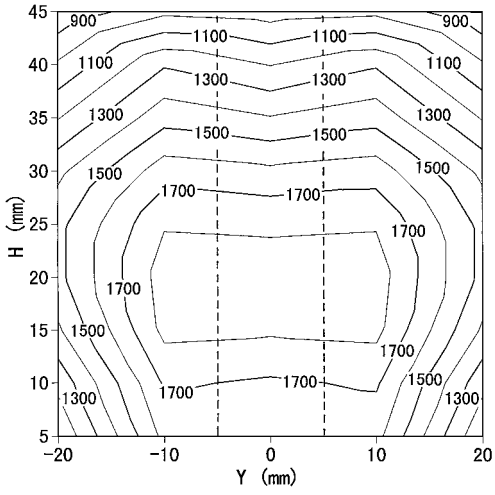

Fig. 11 Temperature profile under high air velocity and low air temperature conditions for parallel fuel injection with pilot fuel injection: $V_{a\,\mathrm{in}}$ = 100 m/s, $T_{a\,\mathrm{in}}$ = 600 K, ϕ_m = 0.36, q = 14, H_n = 5 mm, L = 100 mm, d = 0.7 mm, and T_f = 298 K.

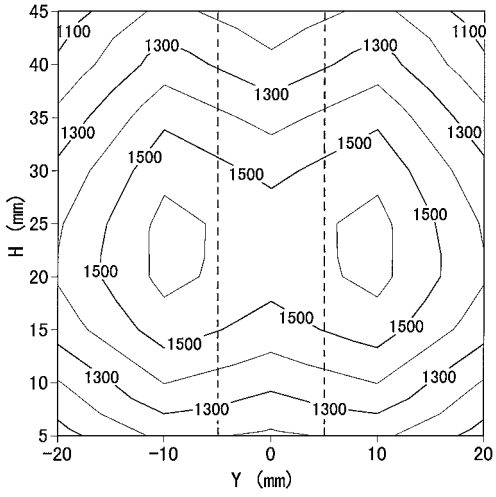

Fig. 12 Temperature profile under low air velocity and high air temperature conditions for parallel fuel injection: $V_{a\,\mathrm{in}}$ = 60 m/s, $T_{a\,\mathrm{in}}$ = 900 K, ϕ_m = 0.37, q = 7.5, H_n = 5 mm, L = 100 mm, d = 0.7 mm, and T_f = 298 K.

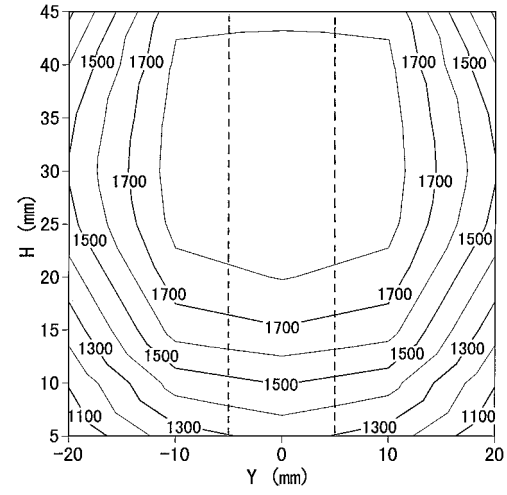

Fig. 13 Temperature profile at a high equivalence ratio: $V_{a\,\mathrm{in}}$ = 60 m/s, $T_{a\,\mathrm{in}}$ = 900 K, ϕ_m = 0.49, q = 13, H_n = 5 mm, L = 100 mm, d = 0.7 mm, and T_f = 298 K.

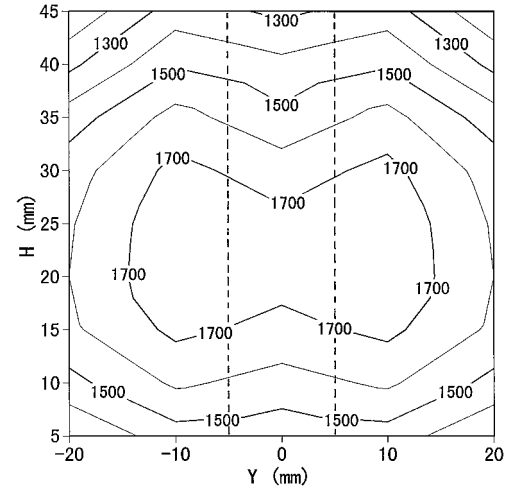

Fig. 14 Temperature profile under low air velocity and high air temperature conditions at low fuel injection temperature: $V_{a\,\mathrm{in}}$ = 60 m/s, $T_{a\,\mathrm{in}}$ = 900 K, ϕ_m = 0.37, q = 7.5, H_n = 5 mm, L = 50 mm, d = 0.7 mm, and T_f = 298 K.

temperature change toward the combustor walls of Fig. 12 is gentler than that in Fig. 11 due to the high inlet air temperature.

Figure 13 shows the temperature profile at a high equivalence ratio of 0.49. The maximum temperature is higher and the high-temperature region is broader than that of the low equivalence ratio condition (see Fig. 12) due to high heat release. The vertical position of the maximum temperature region is higher than that of the low equivalence ratio due to the large fuel-to-air momentum flux ratio. The temperature near the center of the bottom wall is relatively low as compared with that of the high air velocity and low air temperature conditions (see Fig. 11). The high temperature in this region is generally caused by the aforementioned involvement of fuel vapor and fine fuel droplets in the wake region of the fuel injector and the liquid column. Under the conditions in Fig. 13, very few fine fuel droplets are generated near the fuel injector because of low air velocity. Therefore, the equivalence ratio in the wake region decreases and the temperature consequently decreases.

Fuel Temperature

Figures 14 and 15 show the temperature profiles under low air velocity and high air temperature conditions at fuel injection temperatures of 298 and 365 K, respectively. The changes in fuel injection temperature during the experiments were within ±4 K. The maximum temperature at the high-temperature fuel conditions (see

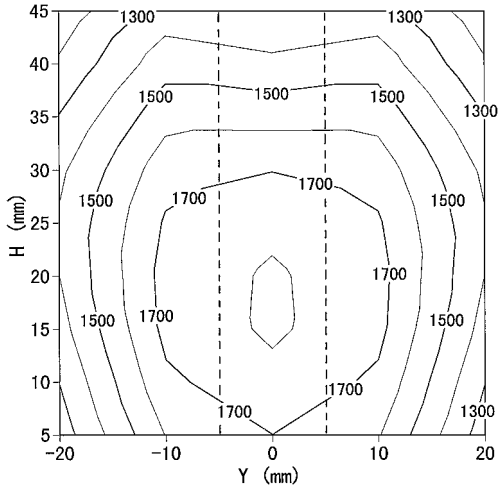

Fig. 15 Temperature profile under low air velocity and high air temperature conditions at high fuel injection temperature: $V_{a\,\mathrm{in}}$ = 60 m/s, $T_{a\,\mathrm{in}}$ = 900 K, ϕ_m = 0.36, q = 7.2, H_n = 5 mm, L = 50 mm, d = 0.7 mm, and T_f = 365 K.

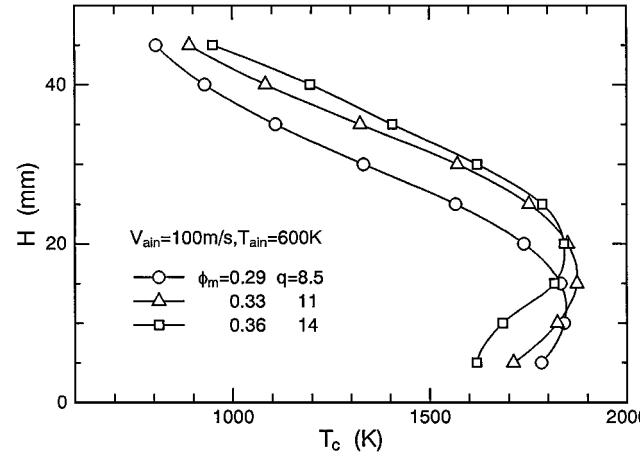

Fig. 16 Temperature distribution along X axis under high air velocity and low air temperature conditions: H_n = 5 mm, L = 100 mm, d = 0.7 mm, and T_f = 298 K.

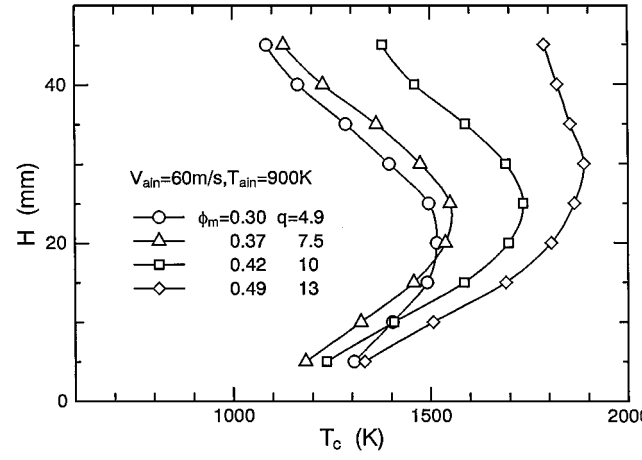

Fig. 17 Temperature distribution along X axis under low air velocity and high air temperature conditions: H_n = 5 mm, L = 100 mm, d = 0.7 mm, and T_f = 298 K.

Fig. 15) is higher than that in the low-temperature fuel conditions (see Fig. 14). This is due to the high initial enthalpy of the high-temperature fuel. The fuel dispersion in the direction of the injection of the high-temperature fuel is lower than that of the low-temperature fuel due to fuel evaporation. This results in the lower vertical position of the maximum temperature in Fig. 15. The amount of liquid fuel that is pushed aside along the surface of the gutter decreases with an increase in fuel temperature due to fuel evaporation. Therefore, the shape of the higher temperature region of Fig. 15 is similar to a circle.

Temperature Distributions Along X Axis

Equivalence Ratio

Figures 16 and 17 show the temperature distributions along the X axis at the combustor exit under different inlet conditions. The X axis is normal to the airflow direction, and the results were obtained for parallel fuel injection along the gutter axis. The temperature distributions in Figs. 16 and 17 are at the exit of the combustor, and they cut across the results given in Figs. 10–15.

Under high air velocity and low air temperature conditions (see Fig. 16), the vertical position of the maximum temperature becomes higher as the equivalence ratio increases. This tendency is similar to the increase in jet penetration due to an increase in the fuel-to-air momentum flux ratio.[9] However, the maximum temperature is almost constant and is independent of the equivalence ratio. Here, relatively fine droplets are generated due to high air velocity. Because these fine droplets evaporate rapidly, fuel dispersion is limited. Consequently, a moderate fuel/air mixture with a local equivalence ratio that is close to the stoichiometric ratio is generated even at a small total equivalence ratio. Observation of the jet atomization process under cold airflow conditions shows that the maximum droplet mass flux is almost independent of the fuel-to-air momentum flux ratio at a downstream position that is somewhat far from the fuel injector.[9] Therefore, the maximum local equivalence ratio becomes independent of the total equivalence ratio. For these reasons, the maximum temperature becomes constant even with an increase in the equivalence ratio.

On the other hand, under low air velocity and high air temperature conditions (see Fig. 17), the larger the equivalence ratio is, the higher the maximum temperature is. Under these conditions, the jet penetration and mean droplet size are relatively large. Large penetration and coarse droplets make the fuel dispersion active and generate a fuel/air mixture with a much lower local equivalence ratio than a stoichiometric ratio at a low total equivalence ratio. With the increase in the total equivalence ratio, the maximum local equivalence ratio of the mixture increases. This results in an increase in maximum temperature with an increase in the total equivalence ratio.

Because the experimental data obtained in this paper are limited, the given conclusions are tentative. To clarify the effects of inlet air temperature on the spray characteristics and combustion characteristics, further atomization and combustion experiments are needed, particularly under high air temperature conditions.

Inlet Velocity and Temperature of Vitiation Air

Figure 18 shows the effects of the experimental conditions on the temperature distribution along the X axis at almost the same momentum flux ratio of 13. At $T_{a\,\mathrm{in}} = 600$ K (see circle and square symbols), the temperature distributions have peaks at the same vertical locations for different air velocities because they have the same liquid-to-air momentum flux ratio. This is similar to the tendency of jet penetration under cold airflow conditions.[9] The maximum temperature at $V_{a\,\mathrm{in}} = 100$ m/s is much higher than that at $V_{a\,\mathrm{in}} = 60$ m/s. For $V_{a\,\mathrm{in}} = 100$ m/s, more fine fuel droplets, which are easily evaporated, are generated, than for $V_{a\,\mathrm{in}} = 60$ m/s. These fine droplets generate the moderate fuel/air mixture and raise the temperature.

At $V_{a\,\mathrm{in}} = 60$ m/s (see triangle and square symbols), the maximum temperature at $T_{a\,\mathrm{in}} = 900$ K is much higher than that at $T_{a\,\mathrm{in}} = 600$ K due to the high equivalence ratio. In addition, the temperature upside of the peak of the former decreases more gradually toward the combustor wall. This indicates that the upward dispersion of fuel under high air temperature conditions is better than that under low-temperature conditions.

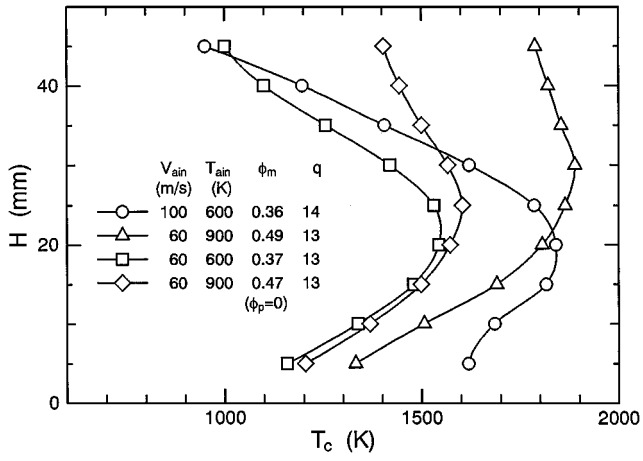

Fig. 18 Effects of experimental conditions on temperature distribution: H_n = 5 mm, L = 100 mm, d = 0.7 mm, and T_f = 298 K.

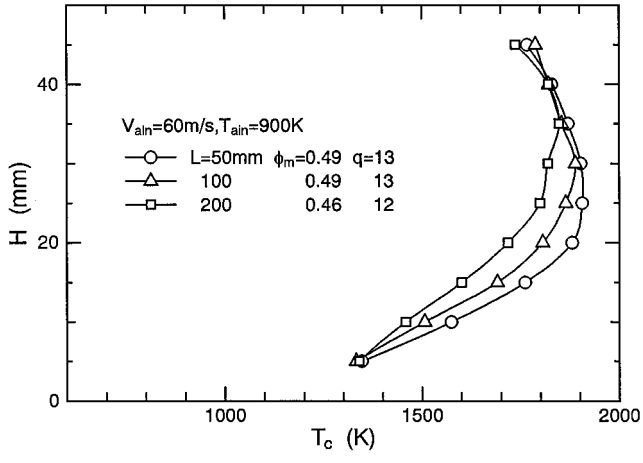

Fig. 19 Temperature distribution along X axis for various horizontal distances between fuel injection and the gutter: H_n = 5 mm, d = 0.7 mm, and T_f = 298 K.

On the other hand, the vertical position where the distribution has its peak at $T_{a\,\mathrm{in}} = 900$ K is higher than that at $T_{a\,\mathrm{in}} = 600$ K. This is due to the large penetration of the fuel jet and droplets at $T_{a\,\mathrm{in}} = 900$ K, as already mentioned.

Under the air temperature conditions employed in this study, the conclusions about fuel dispersion seem to be valid for other values of the liquid-to-air momentum flux ratio as long as the penetration of the fuel jet and the inertia of droplets are dominant in regard to fuel dispersion. However, under other air temperature conditions, the reliability of the conclusions is not clear because of the limited experimental conditions in this study.

In regard to pilot fuel injection, it is clear that it causes the temperature of the combustion gas to be higher (see diamond symbols).

Distance Between Fuel Injector and Gutter

Figure 19 shows the temperature distributions along the X axis for various horizontal distances between the fuel injector and the gutter (see Fig. 5). As the distance increases, the vertical location of the maximum temperature becomes higher. This is due to the increase in jet penetration. In the case of cold flow conditions, the vertical location of the maximum droplet mass flux does not change nor decrease downstream of $Z_h = 100$ mm due to gravity.[9] This is because the momentum in the direction of fuel injection, which the fuel has at the exit of the fuel injector, is lost until it reaches the location of $Z_h = 100$ mm due to the drag that is caused by the airstream. However, in the case of hot airstream condition (see Fig. 19), the momentum of the droplets seems not to be lost even at $Z_h = 200$ mm due to the decrease in the drag that is caused by the airstream.

On the other hand, Wu et al. pointed out that the vertical location of the maximum mass flux increases with the axial distance in the case of smaller jet diameter, for example $d = 0.5$ mm, and larger fuel-to-air momentum flux ratio.[18] The minimum diameter of the injector used in the previous paper is 1 mm (Ref. 9). Thus, it is likely that the vertical location of the maximum mass flux increases with the axial distance under both cold and hot airstream conditions, limited to the case of smaller jet diameter and larger fuel-to-air momentum flux ratio. Further studies of a jet trajectory, however, are required to clarify the causes of the discrepancies of a jet trajectory between conditions of cold and hot airstreams.

The maximum temperature decreases as the distance increases, as is shown in Fig. 19. This is caused by fuel dispersion. As the fuel/air mixture progresses downstream, the maximum local equivalence ratio decreases due to the turbulent fuel dispersion.

Total Pressure Loss

Figure 20 shows the variations of the static pressure measured on the combustor wall. The experimental uncertainties for pressure measurements were estimated to be less than 0.2%. The static pressure near the gutter with combustion is much higher than that without combustion, and the former is greatly reduced downstream because of the increased viscosity and the acceleration of the combustion gases due to heat release. The pressure loss across the recirculation zone behind the gutter with combustion is larger than that without combustion. This conclusion is similar to that pointed out by Lewis and von Elbe.[19] Under combustion without pilot fuel injection, a slight recovery of static pressure behind the gutter can be observed. However, recovery of the static pressure with pilot fuel injection cannot be observed. This phenomenon qualitatively corresponds with the present observation that pilot fuel injection shrinks the recirculation zone behind the gutter.

Figure 21 shows the total pressure loss normalized by the total pressure at the combustor inlet for parallel and perpendicular fuel injections. In Fig. 21 ϕ_t stands for the total equivalence ratio, that is, $\phi_t = \phi_m + \phi_p$. The total pressure losses when $V_{a\,\mathrm{in}} = 100$ m/s and $T_{a\,\mathrm{in}} = 600$ K are significantly larger than those when $V_{a\,\mathrm{in}} = 60$ m/s and $T_{a\,\mathrm{in}} = 900$ K, independent of the geometry of fuel injection used. The total pressure loss due to aerodynamics, therefore, accounts for a major part of the total pressure loss. In both examples, the total pressure losses seem to increase linearly with the increase in the total equivalence ratio except for the examples without combustion because of the increase in heat release due to combustion, as discussed by Saito et al.[20] The total pressure loss through the combustor is less than 6% within the limited range of the present experimental conditions.

In Fig. 21 the combustion efficiencies that are small, especially for perpendicular fuel injection (see Table 3), were not taken in consideration for the calculation of the equivalence ratio. When combustion efficiency is improved, total pressure loss is expected to increase to some extent, especially for perpendicular fuel injection.

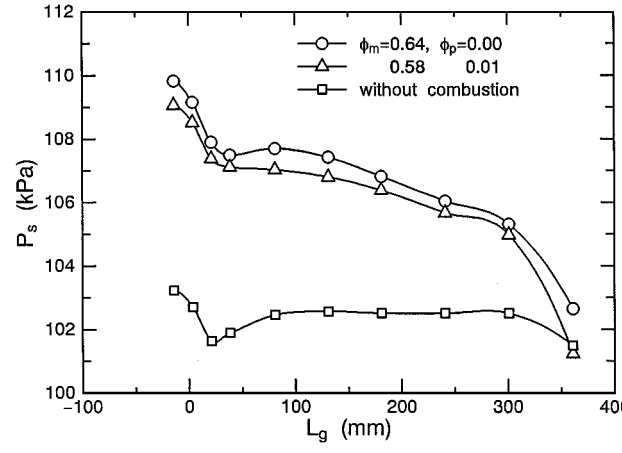

Fig. 20 Static pressure distribution along X axis: $V_{a\,\mathrm{in}}$ = 100 m/s, $T_{a\,\mathrm{in}}$ = 600 K, H_n = 5 mm, L = 100 mm, d = 0.7 mm, and T_f = 298 K.

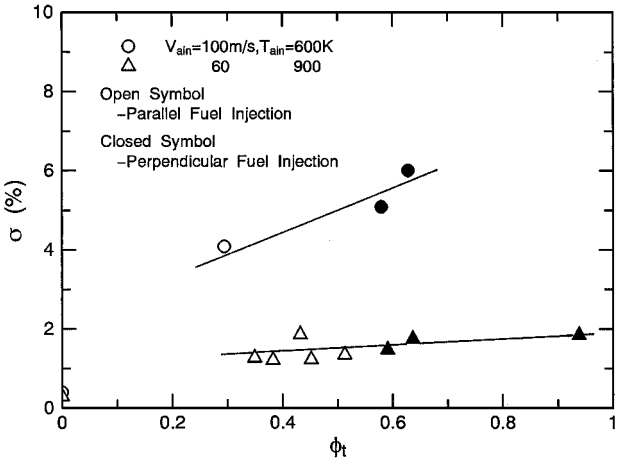

Fig. 21 Normalized total pressure loss with total equivalence ratios: H_n = 5 mm, L = 100 mm, d = 0.7 mm, and T_f = 298 K.

Conclusions

Atomization and combustion tests of a ramjet combustor were carried out to analyze fuel jet penetration and the combustion characteristics of two types of fuel injection. Conclusions can be summarized as follows; although, note that because the experiments were conducted under limited experimental conditions, the following conclusions cannot always be directly applied to conditions in general.

1) The fuel jet penetration in the hot airflow with temperatures of 630 and 903 K and a velocity of around 60 m/s was much larger than that calculated from the empirical equation that was obtained under cold flow conditions in the previous paper.

2) The maximum and minimum equivalenceratios of the example with an inlet air temperature of 600 K and an air velocity of 100 m/s are higher than those of the example with air temperature of 900 K and air velocity of 60 m/s, possibly due to fuel dispersion.

3) The equivalence ratio range under high air temperature conditions with a temperature of 900 K and a velocity of 60 m/s is wider than that under air temperature conditions with a temperature of 600 K and a velocity of 60 m/s due to the promotion of fuel evaporation.

4) Under conditions with an inlet air temperature of 600 K and an air velocity of 100 m/s, the high-temperature region that is higher than 1500 K in the cross section for the parallel fuel injection is broader than that for perpendicular fuel injection. The measured combustion efficiency in the case of parallel injection is higher than that in the case of perpendicular injection.

5) Under conditions with an inlet air temperature of 900 K and an air velocity of 60 m/s, the fuel dispersion in the fuel injection direction of the high-temperature fuel with a temperature of 365 K is lower than that of low-temperature fuel with a temperature of 298 K, possibly due to fuel evaporation.

6) In the present experimental condition range, pilot fuel injection of gaseous hydrogen from the gutter is very effective for improving combustion characteristics.

7) Combustion causes an increase in total pressure loss through the combustor. Under both types of conditions, with an inlet air temperature of 600 K and an air velocity of 100 m/s and with an air temperature of 900 K and an air velocity of 60 m/s, the total pressure loss increases with an increase in the equivalence ratio, and it is limited to less than 6% within the limited range of the present experimental conditions.

Acknowledgments

The authors wish to express their thanks to M. Sasaki, H. Sakamoto, K. Yoshimura, and M. Sei for their help with the experiments.

References

[1]Waltrup, P. J., "Liquid-Fueled Supersonic Combustion Ramjets: A Research Perspective," *Journal of Propulsion and Power*, Vol. 3, No. 6, 1987, pp. 515–524.

[2]Nejad, A. S., and Schetz, J. A., "Effects of Properties and Location in the Plume on Droplet Diameter for Injection in a Supersonic Stream," *AIAA Journal*, Vol. 21, No. 7, 1983, pp. 956–961.

[3]Less, D. M., and Schetz, J. A., "Penetration and Breakup of Slurry Jets in a Supersonic Stream," *AIAA Journal*, Vol. 21, No. 7, 1983, pp. 1045, 1046.

[4]Thomas, R. H., and Schetz, J. A., "Distributions Across the Plume of Transverse Liquid and Slurry Jets in Supersonic Airflow," *AIAA Journal*, Vol. 23, No. 12, 1985, pp. 1892–1901.

[5]Schetz, J. A., and Padhye, A., "Penetration and Breakup of Liquids in Subsonic Airstreams," *AIAA Journal*, Vol. 15, No. 10, 1977, pp. 1385–1390.

[6]Kashiwagi, T., "Study on Afterburner of Aircraft Engine," *Ishikawajima–Harima Engineering Review*, Vol. 31, No. 2, 1991, pp. 109–114 (in Japanese).

[7]Oda, T., Hiroyasu, H., Arai, M., and Nishida, K., "Characteristics of Liquid Jet Atomization Across a High-Speed Airstream (1st Rep.)," *Transactions of the Japan Society of Mechanical Engineers*, Vol. 58, No. 552, 1992, pp. 2595–2606. (in Japanese).

[8]Wu, P. -K., Kirkendall, K. A., Fuller, R. P., and Nejad, A. S., "Breakup Processes of Liquid Jets in Subsonic Crossflows," *Journal of Propulsion and Power*, Vol. 13, No. 1, 1997, pp. 64–73.

[9]Inamura, T., and Nagai, N., "Spray Characteristics of Liquid Jet Traversing Subsonic Airstreams," *Journal of Propulsion and Power*, Vol. 13, No. 2, 1997, pp. 250–256.

[10]Schetz, J. A., Cannon, S. C., and Baranovsky, S., "Ignition of Liquid Fuel Jets in a Supersonic Airstream," *AIAA Journal*, Vol. 18, No. 9, 1980, pp. 1101, 1102.

[11]Vinogradov, V. A., Kobigsky, S. A., and Petrov, M. D., "Experimental Investigation of Kerosene Fuel Combustion in Supersonic Flow," *Journal of Propulsion and Power*, Vol. 11, No. 1, 1995, pp. 130–134.

[12]Tamaru,T., "Prospects of Aviation Engine Combustors for Next Generation," *Nensho Kenkyu*, No. 88, 1991, pp. 1–14 (in Japanese).

[13]Tamaru, T., Shimodaira, K., and Yamada, H., "Combustion Problems on Methane-Fueled Liner Type of Ram-combustor," *Journal of the Gas Turbine Society of Japan*, Vol. 20, No. 79, 1992, pp. 158–164 (in Japanese).

[14]Sjöblom, B., "Full-Scale Liquid Fuel Ramjet Combustor Tests," *International Symposium on Air Breathing Engines*, ISABE Rept. 89-7027, Athens, 1989, pp. 273–281.

[15]Inamura, T., Nagai, N., Yoshimura, K., Kumakawa, A., and Yatsuyanagi, N., "Spray Formation and Spray Combustion in Ramjet Combustor," *Proceedings of the American Society of Mechanical Engineers/Japan Society of Mechanical Engineers Thermal Engineering Joint Conference*, Maui, Hawaii, 1995, pp.157–162.

[16]Lefebvre, A. H., *Atomization and Sprays*, Hemisphere, New York, 1989, pp. 304, 305.

[17]Hsiang, L. -P., and Faeth, G. M., "Near-Limit Drop Deformation and Secondary Breakup," *Multiphase Flow*, Vol. 18, No. 5, 1992, pp. 635–652.

[18]Wu, P. -K., Kirkendall, K. A., Fuller, R. P., and Nejad, and A. S., "Spray Structures of Liquid Fuel Jets Atomized in Subsonic Crossflows," AIAA Paper 98-0714, Jan. 1998.

[19]Lewis, B., and von Elbe, G., *Combustion, Flames and Explosions of Gases*, Academic, New York, 1987, pp. 457–466.

[20]Saito, T., Tamaru, T., Shimodaira, K., Horiuchi, S., and Yamada, H., Hydrogen Combustion Tests Simulating a Subsonic Ram-Combustor for a Hypersonic Plane, *Transactions of the Japan Society of Mechanical Engineers*, Vol. 56, No. 521, 1990, pp. 189–193 (in Japanese).